Stochastic resonance in coupled nonlinear dynamic elements

M. Löcher,[a] D. Cigna, E. R. Hunt, and G. A. Johnson[b]
Department of Physics and Astronomy, Condensed Matter and Surface Sciences Program, Ohio University, Athens, Ohio 45701

F. Marchesoni[c]
Department of Physics, University of Illinois, 1110 West Green St., Urbana, Illinois 61801

L. Gammaitoni
Dipartimento di Fisica, Universita' degli Studi di Perugia and Istituto Nazionale di Fisica Nucleare, Via A Pascoli, I-06100 Perugia, Italy

M. E. Inchiosa and A. R. Bulsara
SPAWAR Systems Center, San Diego, California 92152-5000

(Received 30 January 1998; accepted for publication 11 May 1998)

We investigate the response of a linear chain of diffusively coupled diode resonators under the influence of thermal noise. We also examine the connection between spatiotemporal stochastic resonance and the presence of kink–antikink pairs in the array. The interplay of nucleation rates and kink speeds is briefly addressed. The experimental results are supplemented with simulations on a coupled map lattice. We furthermore present analytical results for the synchronization and signal processing properties of a Φ^4 field theory and explore the effects of various forms of nonlinear coupling. © *1998 American Institute of Physics.* [S1054-1500(98)01503-1]

We extend the phenomenology of stochastic resonance (SR) to arrays of coupled dynamic elements. For correctly chosen parameters, such as coupling and noise strength, the signal-to-noise ratio (SNR) can be significantly enhanced over that of a single element. We demonstrate that for optimized parameters, the greatly improved system response is characterized by a global synchronization of the array and a locally maximized SNR. Furthermore, the system switches phase not concurrently but via the formation of energetically cheaper kink–antikink pairs. We present experimental evidence for all these phenomena and support the findings with results from a coupled map lattice. We conclude with a discussion of the signal processing properties of large arrays of nonlinear dynamic elements, and the effects stemming from different forms of coupling, and global/local noise.

I. INTRODUCTION

Stochastic resonance (SR) is a process in which noise—acting on a nonlinear, multi-stable system, which is modulated by a weak external driving signal—enhances the periodic character of the system response.[1] The output signal-to-noise ratio (SNR) is maximized (SNR_{max}) by a nonzero value of the applied noise. While the notion of SR originated in the context of a single bistable system described by an ordinary (stochastic) differential equation, it was also found to occur in more general systems described by field (partial differential) equations over a decade ago.[2] Only lately though, stochastic resonance in spatially extended systems experienced a surge in research activities.[3–9] In particular, locally or globally coupling the single ''stochastic resonator'' into larger arrays revealed promising results with respect to signal processing abilities.

The term *array enhanced stochastic resonance* (AESR) was recently introduced by Lindner *et al.*[3] to describe spatiotemporal SR in a numerical model of coupled, bistable oscillators. The response of one nonlinear, overdamped oscillator could be further optimized by coupling it locally and linearly into a one-dimensional array of identical oscillators. The SNR_{max} was significantly improved for selected values of the coupling strength and the number of elements in the chain. It was also shown that optimizing the SNR of an individual oscillator coincided with the onset of maximal spatiotemporal synchronization. Scaling laws for the optimum noise intensities and coupling strengths resulting in a maximum SNR as a function of the number of oscillators, N, were derived in Refs. 8, 9. Possible applications for AESR are expected to be found in biological systems and within the area of signal processing.

II. SPATIOTEMPORAL STOCHASTIC RESONANCE IN A SYSTEM OF COUPLED DIODE RESONATORS

A. Array enhancement

In this section we sum up the main results from Ref. 4. We report experimental evidence of AESR in a chain of diffusively coupled nonlinear resonators. The SNR_{max} of the output of one of the middle resonator is observed to increase with the number of elements, here up to 32, for open and periodic boundary conditions. Both the optimal noise inten-

[a]Current address: School of Physics, Georgia Institute of Technology, Atlanta, Georgia 30332. Electronic mail: markus@acl.gatech.edu
[b]Now at Sachs, Freeman, and Associates, Inc., Largo, Maryland 20774.
[c]Also at the Instituto Nazionale di Fisica della Materia, Universita' di Camerino, I-62032 Camerino, Italy.

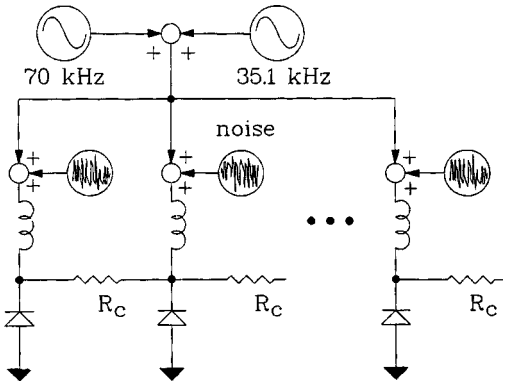

FIG. 1. The circuit diagram sketching the individual noise sources and the 2nd drive added to the main drive. Each diode resonator consists of a diode and an inductance in series. The diffusive coupling is realized via the coupling resistor R_C. The coupling strength is roughly proportional to $1/R_C$.

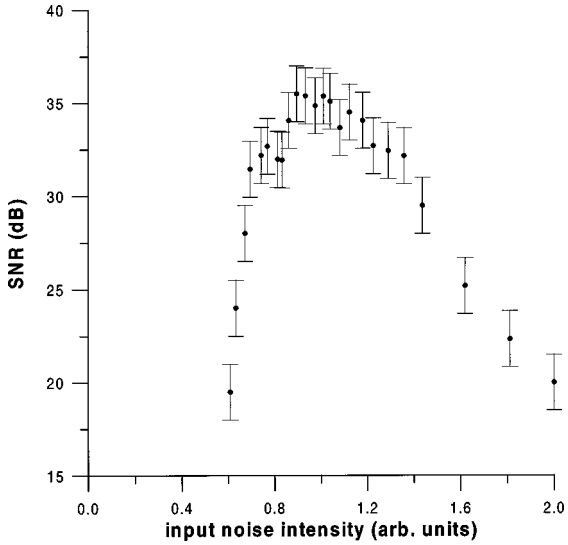

FIG. 2. SNR versus noise power for a single diode resonator. The sharp increase and the following decrease of the SNR are characteristic for stochastic resonance.

sities as well as the optimal coupling strength grow with the length of the array. The array enhancement is most discernible when the resonators are fairly identical. In the experimental setup, the variation in the depth of the potential wells is slightly less than 10%. We experimentally verify that global spatiotemporal synchronization coincides with optimized local performance of a single element in the chain. It is furthermore demonstrated that spatial correlation lengths are maximized by a nonzero noise power analogous to the behavior of the SNR.

For the bistable element we choose the diode resonator, which follows the period doubling route to chaos.[10] The global, sinusoidal drive serves as a bifurcation parameter. By operating in the stable period-2 regime, the two (equally stable) phases give rise to the bistability. We break the phase symmetry by adding a secondary drive signal of half the primary drive frequency, rendering one phase more stable. Phase switching can be induced if (i) the frequency of the added signal is not exactly half the drive frequency, giving rise to a slow beat, and (ii) the amplitude of this resulting low-frequency modulation signal is larger than some threshold. If the amplitude of the modulation signal is chosen below the switching threshold, additional noise is necessary to cause phase jumps. We note that similar symmetry breaking driving signals were utilized in Refs. 11 to achieve phase and trajectory selection. A block diagram of the symmetrically coupled diode resonators is given in Figure 1. The next-neighbor coupling is realized via the coupling resistors R_C. In previous work[12] the coupling strength was found to be roughly proportional to $1/R_C$. The frequencies of the main drive and the second drive are fixed at 70 kHz and 35.1 kHz, respectively, resulting in a beat frequency of 100 Hz. The signals are virtually noise-free within the accuracy of instrument precision, i.e., the amount of correlated noise in the array is negligible. (For an interesting discussion on the interplay between internal and external noise in ensembles of nondynamical elements, see the last reference in Ref. 6.) This situation is in close analogy to arrays of phase-locked loops in antennae which can be assumed to be practically free of correlated noise but are exposed to spatially uncorrelated fluctuations.

We operate the secondary drive at roughly two thirds of the switching threshold amplitude, so that the resonators are confined to one phase if no noise is added. Note that this does not correspond to the weak forcing limit and thus cannot be treated utilizing linear response theory. A different noise source is used for each site, so that there is zero noise correlation between sites. The individual noise sources are far from identical; the standard deviation in the voltage fluctuations between sites is around 10%. The noise is obtained by amplifying shot noise generated by a current through a pn junction diode, and exhibits a flat power spectrum up to at least 100 kHz. The noise intensity is measured in two different ways throughout this paper: *input* intensity (''arb. units'') represents the average of the 32 noise sources and is equal to 2.3×10^{-19} V^2/Hz. *Output* intensity is obtained by taking the power spectrum and measured in dB. We process the current through the diode from the middle resonator of the array with a dynamic signal analyzer in order to compute the power spectra. The SNR is calculated by measuring the signal power in dB at 100 Hz and subtracting the noise power in the immediate vicinity of the signal. For accuracy the power spectrum is averaged over 20 measurements.

Stochastic resonance in a single system is characterized by a maximum in the SNR curve as the noise power is varied. A typical SNR curve is presented in Figure 2, clearly showing the so-called ''fingerprint of stochastic resonance:'' a sharp rise to a maximum SNR at a finite noise intensity and a subsequent slow decay of the SNR towards higher values of noise.

In the case of an array there are two additional dimensions in parameter space to be mapped out: the coupling strength as well as the number of elements. In Figure 3, the maximum SNR's for a fixed number of diode resonators (eleven) and various coupling strengths are plotted versus input noise intensity. Note that smaller values of R_C result in stiffer coupling. The horizontal bars are a measure of the width of the peaks of the SNR curves. For optimal coupling

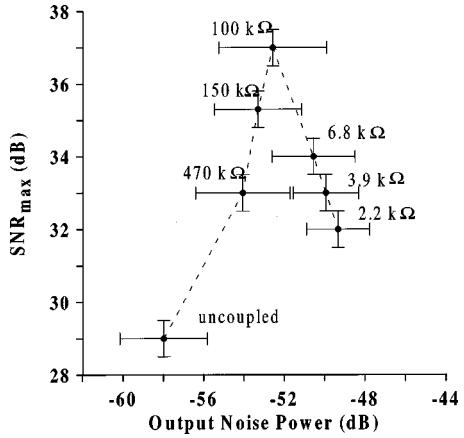

FIG. 3. Maximum SNR of the middle oscillator ($N=11$) for seven different coupling strengths. With optimum coupling, in this case $R_C=100$ kΩ, the SNR of eleven diode resonators surpassed the SNR of a single element by roughly 8 dB. The horizontal bars are a measure of the width of the peaks.

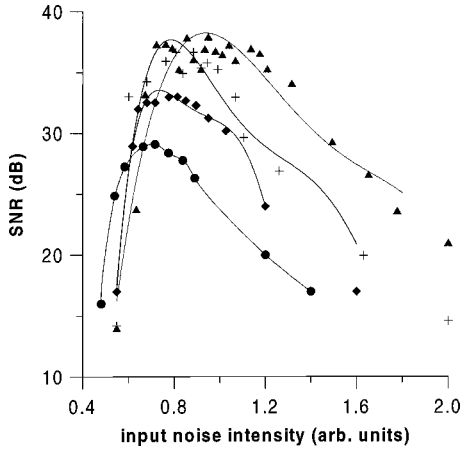

FIG. 4. SNR curves for different numbers of resonators. From top to bottom: $N=32,11,3,1$. The respective coupling strengths are optimized. The curves and their peaks are seen to broaden with an increasing number of elements.

(in this case 100 kΩ) the peak was very broad. Two main tendencies found in Ref. 3 are verified here. As the coupling becomes more and more rigid, (i) SNR_{max} is assumed at higher noise intensities, and (ii) its value initially rises, peaks at some intermediate coupling strength and abates.

Intuitively, (i) and (ii) can be understood in the following way.[3,5] With stiffer coupling, the chain behaves more and more like a rigid rod, so that a greater fraction of oscillators switch phase synchronously. But the intensity of the sum of N uncorrelated Gaussian noise sources scales like $\sqrt{N}$, thus requiring higher noise intensities at the individual sites as either N or the coupling increase. As pointed out by Collins *et al.*,[6] not only does the SNR peak shift to higher noise intensities but it also broadens significantly as the number of elements is growing. In their numerical simulation, the individual, *uncoupled* sites of the array were represented by models of neurons, whose outputs were simply added. Though conceptually different in design—excitable neurons instead of bistable oscillators and no coupling parameter—we found evidence for a widening of the peak as well. Figure 4 displays the SNR curves for various array sizes, optimized over coupling. The tails of the graphs are seen to fall off notably less rapidly for a higher number of resonators. We believe that this effect is also due to the fact that the noise sources are independent, hence partially cancelling each other, whereas the signal power is being added coherently.

In Figure 5 we plot the enhancement in SNR_{max}, maximized over noise, versus coupling strength for some of the different array sizes we examined.

The reference value of zero thus corresponds to the maximum SNR achieved with a single diode resonator. The increase in SNR_{max} occurs rather markedly for three sites and appears to saturate with higher numbers. For very low as well as for very high coupling, the SNR_{max} of the chain approaches the one for a single oscillator, as discussed above.

For 32 oscillators the maximum enhancement we were able to achieve was 9.5 dB. Only 7 oscillators were sufficient to increase the maximum SNR by 8 dB. The optimal coupling resistor for 32 oscillators was found to be $R_C=15$ kΩ, compared to $R_C=120$ kΩ for 3 resonators. Since the coupling strength scales like $1/R_C$, this corresponds to an eight times stronger coupling.

When applying the noise globally to five resonators, we do not find any coupling enhancement, which appears in agreement with conclusions from earlier numerical simulations.[8,9] The effect of different boundary conditions is most notable for low numbers of oscillators. When employing periodic boundary conditions with just three oscillators, the maximum reachable SNR is slightly lower and shifts towards weaker coupling. Intuitively, the *effective* coupling is lower for open boundary conditions than for a closed loop, explaining the shift. Already for 7 and 11 oscillators no dependence on the boundary conditions could be detected.

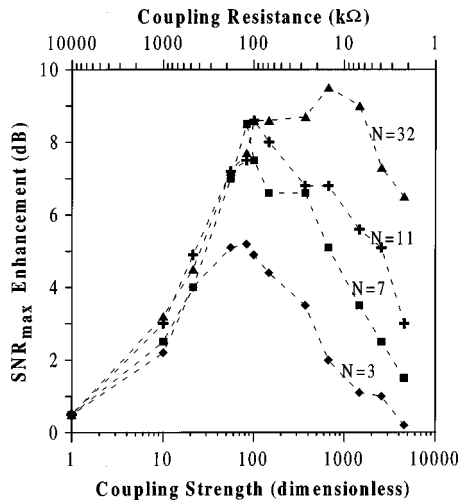

FIG. 5. Maximum SNR enhancement, maximized over noise, is plotted against the coupling strength. To aid the eye the symbols are connected with dotted lines. The different lines correspond to the different number of resonators. For clarity the graph for $N=5$ was omitted. Larger arrays clearly enhance the maximum SNR.

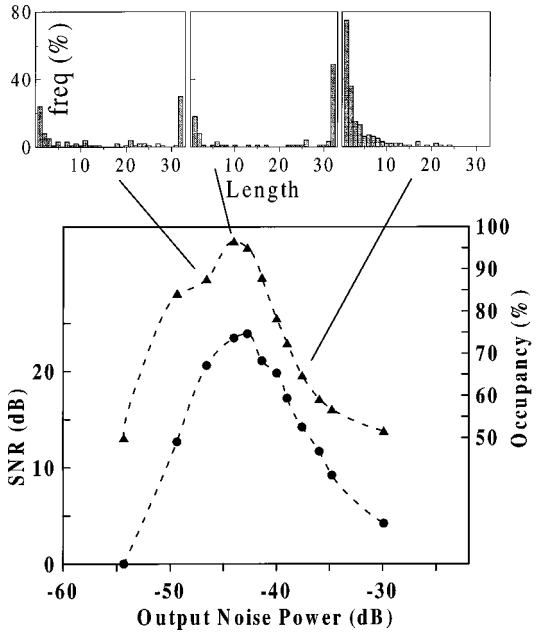

FIG. 6. Occupancy (△) and SNR (○) for 32 resonators versus noise power (periodic boundary conditions). Note that for this plot the intrawell motion was discarded, so that the SNR truly approaches zero for low noise power. The coupling resistor was chosen to be optimal, $R_C = 15\ \mathrm{k}\Omega$. The histograms display the distribution of domain length scales, at noise powers 1.35, 1.6, and 2.3 (from left to right). The arrows indicate the corresponding values of occupancy/SNR. Each histogram is comprised of about 200 data points.

B. Global vs local dynamics

The emphasis so far has been on the performance of a single element in the array. In order to obtain a more global perspective connecting the local dynamics to the behavior of the entire array, we adopt the notion of the *occupancy* function, which was introduced in Ref. 3. It constitutes a measure of the average spatiotemporal synchrony and is defined as the percent of resonators assuming the preferred phase at the extremes of the modulation signal. The *extremes* of the modulation signal are understood as the two unique phases of the beat frequency which result in maximum asymmetry in the size of the two basins of attractions. The respective values were inferred experimentally by choosing the amplitude of the secondary drive to lie barely above the threshold and measuring the phase of the beat at the instant of a phase jump.

By definition, an occupancy value of 100% corresponds to perfect spatial **and** temporal synchronization, whereas 50% occupancy can be caused by either complete spatial disorder (high noise power) or by a spatially uniform chain of resonators confined to one phase (low noise limit). We measure the occupancy function using a device that periodically samples the state of all resonators simultaneously and then provides a sequential analog output of the states. This output contains information on correlation lengths, and its time average is a measure of the occupancy function.

Figure 6 clearly demonstrates the strong correlation between the locally measured SNR and the globally determined occupancy. The graphs almost mirror each other and peak at the same noise power, thus verifying that maximum SNR coincides with optimal spatiotemporal synchronization of the array.[3–5,8,9]

While the occupancy function is an efficient, combined measure for spatial and temporal correlations, it hides some of the more subtle, purely spatial features. In particular, we are interested in length scales, i.e., distributions of domain lengths, where *domains* are contiguous blocks of in-phase resonators. The three histograms in Figure 6 illustrate the change in dominant length scales as the noise is varied. The histograms have to be interpreted with caution: the frequencies reflect the occurrence of domain lengths per temporal snapshot which naturally favors shorter lengths. In order to obtain the probability of detecting a particular length at a random site the frequencies have to be rescaled with weights proportional to their respective domain lengths.

Low but finite noise power overcomes the coupling only sporadically, giving rise to a dominant peak at bin 32 and rather low frequencies for smaller domain lengths (the far left histogram). For intermediate/optimum noise strength the peak at bin 32 is even more pronounced, and shorter domain lengths are almost entirely absent. The probability to detect a domain length $\geqslant M$ at a random site at a random time might serve as a convenient quantifying measure for spatial correlation. For $M = 32$, this probability increases from 60% to 80% from the far left histogram to the middle one.

This counterintuitive behavior—adding more noise actually increases spatial correlation—could be viewed as the spatial analogy to ''temporal'' stochastic resonance in a single system where a temporal correlation function is maximized by a finite noise power. High noise intensity leads to very short spatial correlations, which is confirmed in the far right histogram.

III. KINK–ANTIKINK NUCLEATION IN A ϕ^4 MODEL

It was shown by Marchesoni and coworkers[5] that in the limit of strong coupling the discrete system of coupled Duffing oscillators from Ref. 3 approaches the dynamics of the ϕ^4 model. Scaling laws were derived in a subsequent paper[8] which confirmed the analogy between the discrete setup and the continuous ϕ^4 field theory. The phenomenon of AESR and its associated kink–antikink dynamics does not depend on the exact form of the local bistable potential. Hence, for strong coupling we expect to observe very similar phenomenology in the experimental setup. The present section summarizes the results from Refs. 5, 13 and is intended as a tutorial overview of kink nucleation theory. In Sec. IV we present qualitative evidence for the validity of the kink–antikink picture in the experiment. It serves as the connecting thread between the abstract ϕ^4 model and the system of coupled nonidentical diode resonators.

In the continuum limit, a ϕ^4 model is described by the differential equation

$$\phi_{tt} - c_0^2 \phi_{xx} + \omega_0^2 V'[\phi] = -\alpha \phi_t + \zeta(x,t) + F, \tag{1}$$

where $V[\phi] = (1/8)(\phi^2 - 1)^2$ and $\zeta(x,t)$ denotes a Gaussian noise source with spatiotemporal correlation $\langle \zeta(x,t)\zeta(x',t')\rangle = 2\alpha kT\delta(x-x')\delta(t-t')$. The ϕ^4 theory is known to bear both extended (phonons) and localized

(soliton) solutions. Localized solutions can be conveniently reproduced as a linear superposition of uniformly moving kinks, ϕ_+, and antikinks, ϕ_-, with[14]

$$\phi_\pm(x,t)=\tanh\left[\pm\frac{1}{2d}\frac{x-X_\pm(t)}{\sqrt{1-\dot{X}_\pm^2(t)/c_0^2}}\right], \tag{2}$$

provided that the separation between their centers of mass $X_\pm$ is very large compared with their size $d\equiv c_0/\omega_0$ (dilute gas approximation). The equilibrium kink (antikink) density in the symmetric ($F=0$) ϕ^4 model at finite temperature is known,[14]

$$n_\pm=n_0=\left(\frac{3}{2\pi}\right)^{1/2}\frac{1}{d}\left(\frac{E_0}{kT}\right)^{1/2}\exp(-E_0/kT), \tag{3}$$

where $E_0=(2/3)\omega_0 c_0$ is the rest energy and $M_0=E_0/c_0^2$ is the mass of $\phi_\pm$. It follows that the dilute gas approximation holds for $n_0^{-1}\gg d$, that is at low temperatures, $kT\ll E_0$. In such a regime, $\langle\dot{X}_\pm^2\rangle=kT/M_0\ll c_0^2$, so that the relativistic boost factor in Eq. (2) may be approximated to unity.

The perturbation forces $\zeta(x,t)$ and F cause a rigid translation of the kink (antikink) against which $\phi_\pm$ is in neutral equilibrium. In other words, the shape of $\phi_\pm$ is not affected by the perturbation, whereas its center of mass coordinate is replaced by a random variable $X_\pm(t)$. In the overdamped limit, $\alpha\gg\omega_0$, a single kink (antikink) undergoes a driven Brownian motion described by the Langevin equation,[13,15]

$$\dot{X}_\pm=\mp 2F/\alpha M_0+\eta(t), \tag{4}$$

where $\eta(t)$ is a Gaussian, zero-mean valued random force with correlation function $\langle\eta(t)\eta(0)\rangle=2(kT/\alpha M_0)\delta(t)$: the static forcing term F pulls $\phi_\pm$ in opposite directions with average speed

$$u_\pm=\langle\dot{X}_\pm\rangle=\mp 2F/\alpha M_0. \tag{5}$$

The elementary mechanism which allows a ϕ^4 chain to switch between its vacuum configurations $\phi=\pm 1$ is the *nucleation of kink–antikink pairs*. Thermal fluctuations are expected to trigger the process by activating a critical nucleus, the size of which may be shown to increase with decreasing F. Provided that the size of the critical nucleus is small enough to ignore many-body effects[16] due to the equilibrium kink–antikink gas with density (3), we can describe the nucleation process as a local two-body process: *the relevant saddle-point configuration is represented by such a critical nucleus and not by the unstable homogeneous solution* $\phi=0$! This introduces a spatial correlation length in the chain switching mechanism.

The nucleation rate Γ, defined as the number of kink–antikink pairs nucleated per unit of time and length, can be calculated analytically in the limits of strong damping, $\alpha\gg\omega_0$, and low temperature, $kT\ll E_0$, introduced above. For simplicity, we assume that the chain sits initially in the stable homogeneous state $\phi_0(x)=-1$ and that the forcing term F is constant and positive definite. A large nucleus $\phi_N(x,X)$ with length $2X\gg d$ is well represented by the linear superposition of a kink and an antikink centered at $\mp X$, respectively,

$$\phi_N(x,X)=\phi_+(x+X,0)+\phi_-(x-X,0)+1. \tag{6}$$

Here the center of the nucleus has been set at the origin without loss of generality. Its components experience two contrasting forces: an attractive force due to the vicinity of the nucleating partner and a repulsive force due to the external bias F. In view of Eq. (6), the potential function corresponding to the internal force is[5]

$$\begin{aligned}V_N(X)&=\int_{-\infty}^{+\infty}H[\phi_N(x,X)]dx\\&=6E_0[(-2/3+3K-2K^2)+(X/d)(1-3K^2-2K^3)],\end{aligned} \tag{7}$$

with $K=\tanh^{-1}(X/d)$ and for $X\gg d$ may be further approximated to

$$V_N(X)=2E_0[1-6\exp(-2X/d)]. \tag{8}$$

The potential of the external force F can be determined by integrating the drift term of Eq. (4), that is $\pm 2FX$. The *critical* nucleus configuration $\phi_N(x,R)$ is attained for a relative kink–antikink distance, $2R(F)$, such that the two competing forces compensate each other, i.e., for

$$2R(F)=-d\,\ln(Fd/12E_0), \tag{9}$$

and decays through one unstable mode, only—the collective variable $X(t)$—with negative eigenvalue

$$\lambda_0^N=V_N''(R)/M_0=-4F/M_0 d. \tag{10}$$

Moreover, its energy $\Delta E_N(F)$ is obtainable through Eq. (8) after replacing X with $R(F)$.

In the Gaussian approximation, the nucleation rate for the biased *overdamped* ϕ^4 chain is given by Langer's formula,[13,15]

$$\Gamma_2=\frac{|\lambda_0^N|}{2\pi}\frac{Z_N}{Z_0}\exp(-\Delta E_N/kT), \tag{11}$$

where Z_0 and Z_N denote the (subtracted) partition function for the vacuum and the critical nucleus field configuration, respectively. The entropic factor Z_N/Z_0 accounts for both the phonon modes (with continuum spectrum), which ''dress'' $\phi_0(x)$ and ϕ_N, and the two internal modes of ϕ_N with discrete (nearly degenerate) eigenvalues $\lambda_b^N=\sqrt{3}\omega_0/2$.[14] A standard calculation yields the following analytical expression for Γ_2:[5]

$$\Gamma_2=\frac{9}{\pi}\frac{\omega_0^2}{\alpha d}\left(\frac{F}{3\pi}\right)^{1/2}\left(\frac{\Delta E_N}{kT}\right)^{1/2}. \tag{12}$$

The validity of Eq. (12) is restricted by the condition that $kT/E_0\ll F/\omega_0^2\ll 1$ (strong bias regime). The inequality $F\ll\omega_0^2$ corresponds to requiring that the tilted ϕ^4 potential $\omega_0^2 V[\phi]-F\phi$ retains its bistable nature and, more importantly, that the relevant offset of $\phi_\pm$ in Eq. (2) may be ignored. As a matter of fact, that would amount to rescaling $\omega_0\to\omega_0\sqrt{1-F/\omega_0^2}$ or, equivalently, for the stationary speed of the driven kink (antikink),[17]

$$u_\pm\to u_\pm/\sqrt{1-F/\omega_0^2}. \tag{13}$$

Note that this ''concavity'' in the kink speed is observed experimentally (see Sec. IV A and Fig. 9) and in the model (see section V C and Fig. 14).

The inequality $Fd \gg kT$ is implicit in Langer's derivation of formula (11). In Ref. 13 the two-body model has been solved without having recourse to the Gaussian approximation: the corrected formula for the nucleation rate in the weak bias regime $kTn_0(T) \ll F \ll kT/d$ reads as

$$\Gamma_1(F) = \Gamma_2(F)\kappa(F), \tag{14}$$

with

$$\kappa(F) = 2\pi\sqrt{\frac{Fd}{\pi kT}} \tag{15}$$

and $\Delta E_N(F) \sim 2E_0$. This second expression for Γ is compatible with the linear response theory requirements[16] and can be cast in a more suggestive form, namely,

$$\Gamma_1 = 2(2n_0(T))^2|u_\pm|. \tag{16}$$

Equation (16) is the kinetic model prediction for the nucleation rate in an overdamped ϕ^4 theory.[13]

The reason for switching from Γ_2 to Γ_1 lends itself to a direct experimental verification (see Fig. 15, below). In the Gaussian approximation the nucleation mechanism is controlled essentially by thermal activation; the decay time of the critical nucleus is taken to be finite and negligible with respect to the activation time. In the weak bias regime, however, the parabolic approximation (10) is not accurate[15] and the nucleus decay is better described as a steady downhill sliding motion with speed $|u_\pm|$; the nucleation process is then deemed accomplished only after the nucleating partners have covered a distance of the order of the mean free path $n_0(T)^{-1}$. Finally, for $F \ll kTn_0(T)$ many-body effects become dominant and the critical nucleus picture is of no use.[16]

IV. NUCLEATION OF KINK–ANTIKINK PAIRS IN THE EXPERIMENT

While not intended to serve as a rigid experimental verification of the universality of the findings for the ϕ^4 model derived in the previous section, Figure 7 provides strong supporting evidence for the above summarized arguments. In order to demonstrate the various widths of nuclei for different coupling strengths, we operate in a noise free, subthreshold drive region and induce a kink–antikink pair at site 16 in the following way. The amplitude of the 2nd drive at site 16 was increased until phase switching occurred. Note that we are not able to make any statements about the size of the *critical* nucleus since this is a forced nucleation. For loose coupling the transitions are very sharp, and the width of the nucleus is seen to be only a fraction of the lattice length (Fig. 7a). If the coupling is chosen to be rather tight (Fig. 7c), the kink–antikink pair extends well beyond the system boundaries. The shape of the nucleus in the case of optimum coupling is illustrated in the graph b. The width of the nucleus, defined as the distance between the centers of the kink/antikink, is of the order of half the chain. The corresponding SNR is significantly higher than in the cases of a and c.

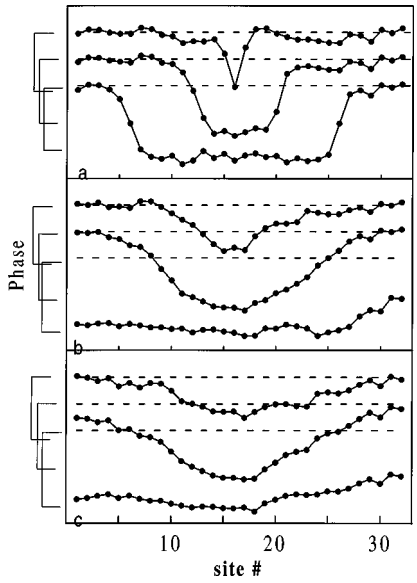

FIG. 7. Each graph contains three snapshots of the 32-resonator chain demonstrating the formation and spreading of a kink–antikink pair for three different coupling strengths and open boundary conditions. The curves are staggered with time evolving downwards. The brackets indicate the extremes of the phase. The kink/antikink widths are seen to vary dramatically with coupling strength: loose coupling in a ($R_C = 180$ kΩ), tight coupling in c ($R_C = 3.9$ kΩ), and optimal coupling for b ($R_C = 15$ kΩ). The SNR's of a and c are 2.2 dB below the one achieved with the configuration b.

In order to see how kink–antikink pairs are nucleated in a noisy environment, Figure 8 shows staggered snapshots of the thermal nucleation and subsequent spreading of a kink–antikink pair.

In the hope of gaining more insight into the dynamics of the hopping process of the array for various coupling and noise strengths we examine two significant time scales in more detail: (i) the speed of each component of a nucleating pair as a function of forcing amplitudes and (ii) the kink nucleation rates as a function of temperature,[18] both for a range of coupling strengths. For the remainder of this section, the number of resonators is fixed to 32, and periodic boundary conditions are employed.

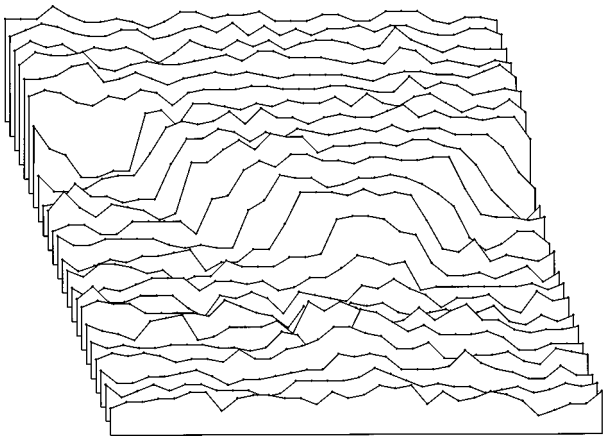

FIG. 8. Shown are staggered snapshots of the 32-resonator chain demonstrating the thermal formation and subsequent spreading of a kink–antikink pair. The curves are separated by eight drive cycles with time evolving upwards. The employed coupling resistor is 68 kΩ.

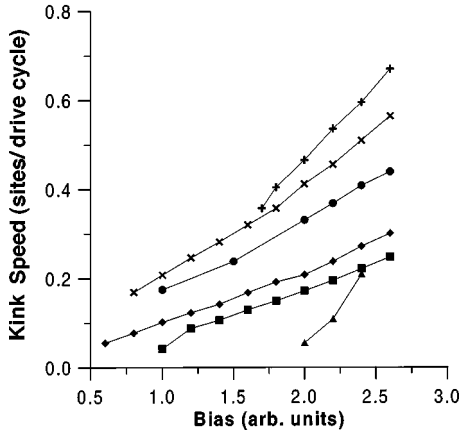

FIG. 9. Kink speed as a function of force for various coupling strengths. From top to bottom: $R_C = 6.8\ \mathrm{k}\Omega$, 15 kΩ, 27 kΩ, 68 kΩ, 100 kΩ, 180 kΩ. (Note that the coupling strength is *inversely* proportional to the value of the coupling resistors.) The force is a measure of the asymmetry of the basin of attraction of the two phases. The curves are well fit by a straight lines. For low coupling strength and low forcing, kinks can get trapped due to discreteness effects and inhomogeneities.

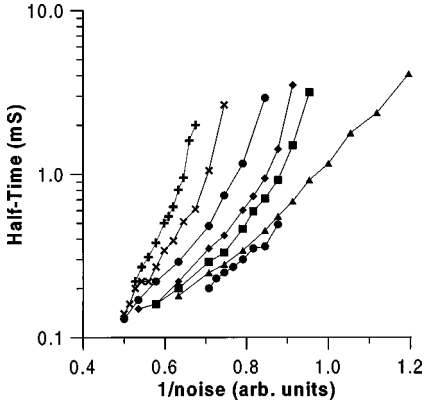

FIG. 10. Half-time (as defined in the text) as a function of inverse noise intensity, for various coupling strengths: From left to right: $R_C = 6.8\ \mathrm{k}\Omega$, 15 kΩ, 27 kΩ, 68 kΩ, 100 kΩ, 180 kΩ. Two regions can be separated in which the curves are approximately linear, each with a different slope. Note that the coupling strength is *inversely* proportional to the value of the coupling resistor.

In the continuum case of the overdamped ϕ^4 theory, the motion of a kink was shown to be a driven Brownian walk, where the deterministic part of the velocity depends linearly on the forcing amplitude; see Eq. (5) in Sec. III. It is quite educational to compare this theory with the case of coupled (i.e., discrete), nonidentical elements. Figure 9 shows the measured kink velocities in the experimental setup (in a noise free environment) for a broad range of coupling resistors. A linear relationship can clearly be verified over an intermediate range of force values. For low values of the coupling strength both discreteness effects and inhomogeneities slow down the kink propagation. The inhomogeneities arise because the elements are not identical and the noise intensity has a non-negligible variation from site to site. Thus, the local ''barriers,'' i.e., the energies needed to induce a transition vary significantly, which leads to kink trapping. Discreteness effects also affect kink speeds for low enough forcing, even if all elements are identical. The model—which is developed later in this article—shows a finite cutoff for the velocity at low coupling strengths due to its discrete nature; see Figure 14. Also, nonlinear effects for higher forcing can be recognized both in Figure 9 as well as later in the model. A nonlinear rescaling of the kink speed is predicted by the ϕ^4 theory; see Eq. (13). For forcing values higher than ~ 2.6 inhomogeneities lead to multiple kink nucleation corrupting the measurements. The curves in Figure 9 corresponding to the extreme coupling values, 6.8 kΩ and 180 kΩ, should be evaluated with caution: For very weak coupling ($180k$) the kink would move only for relatively strong forcing, while for strong coupling ($6.8k$) it is impossible to nucleate a kink at all in case of low forcing.

As one would expect, the time it takes for a kink–antikink pair to travel around the loop is much shorter than one drive period. (In this case for the beat frequency of 100 Hz and the forcing amplitude used in the SNR measurements as described above.) How does this time relate to the average time it takes to nucleate the first critical nucleus T_{nuc}? In the experiment we are not able to get an accurate measurement of T_{nuc}; instead we can measure average decay times, i.e., the time it takes for the whole chain to decay from its metastable phase into the stable phase. Assuming that the decay-time *after* a kink–antikink pair was created (this time depends inversely on the kink speed) is small compared to the time it takes to nucleate the first pair, a good estimate for T_{nuc} will be half the average (total) decay time. Of course, this approximation breaks down for high noise intensities since the nucleation rate then becomes comparable to the kink speed. We remark that the total decay time is the multidimensional equivalent of the inverse Kramers rate for a single system. Figure 10 shows this half-time as a function of inverse temperature.[18] A step force of 2 units (see Figure 9) is applied to the chain of diode resonators initially being in the energetically less favorable phase. We then measure the average decay rates into the stable phase and plot the (average) time it takes for *half* the elements to switch phase. The curves are roughly piecewise linear on the logarithmic scale, indicating an exponential law in each of the two sections.

V. SPATIOTEMPORAL STOCHASTIC RESONANCE IN A SYSTEM OF COUPLED LOGISTIC MAPS

A. Stochastic resonance in the logistic map

As a low-dimensional dynamical system exhibiting the period doubling route to chaos, the diode resonator is known to be modeled fairly well by a one-dimensional quadratic map.[10] Well established in previous work[12] we choose a chain of (symmetrically) coupled logistic maps as a computationally efficient representation of the experimental setup:

$$x_{n+1}^i = (1-\epsilon) f(x_n^i, r) + \tfrac{1}{2}\epsilon [f(x_n^{i-1}, r) + f(x_n^{i+1}, r)] + D\zeta^i \qquad (17)$$

$[i \in [1,N],\ n \equiv \text{time},\ f(x,r) = rx(1-x),\ x \in (0,1)]$. The adjustable parameter D alters the intensity of the normally distributed deviate ζ^i which has zero mean and unit variance[19] and is independent from site to site.

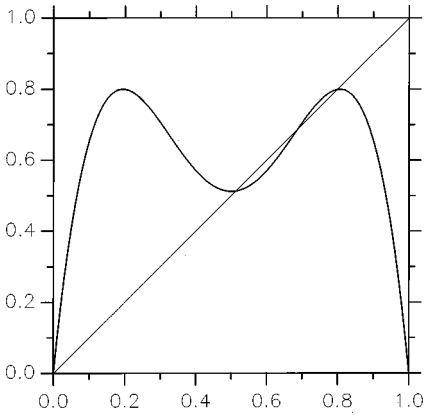

FIG. 11. The 2nd return map with no modulation, $\delta r=0$ ($r=3.2$).

We remark that stochastic resonance in maps and coupled map lattices of a different nature is treated in detail in Ref. 20. In analogy to the experiment, the nonlinearity r is selected to lie within the stable period-2 regime of the logistic map, giving rise to a bistability via the two symmetric phases. Since the value of r corresponds to the amplitude of the main drive of the diode resonator, the ''modulation signal'' is added to this parameter in the following way.

The phase symmetry is broken by a period-2 modulation of r (equivalent to the 35 kHz component of the 2nd drive):

$$r\equiv r_n=\begin{cases} r_0+\delta r, & \text{for } n \text{ even},\\ r_0-\delta r, & \text{for } n \text{ odd},\end{cases}$$

enlarging the size of the basin of attraction of one of the two fixed points of $F(x,r_1,r_2)\equiv f(f(x,r_1),r_2)$ on the expense of the other. Again, this method of symmetry breaking is in close conceptual analogy to previous work by Yang *et al.*[11] Figures 11–12 serve to illustrate the change in the sizes of the basins of attractions. Figure 11 shows the 2nd return map of the logistic map with no modulation. A moderate modulation is applied in Figure 12 resulting in an asymmetry in the basin of attraction size. The phase slip occurs when δr is sufficiently big so that one of the basins entirely disappears.

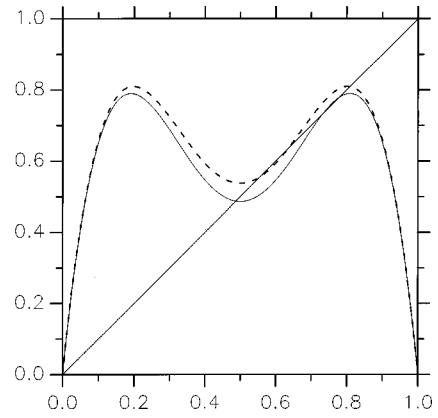

FIG. 12. The 2nd return map with modulation, $\delta r=0.04$, illustrating how the basin of one fixed point grows at the expense of the other ($r=3.2$). The phase determines which return map is obtained; first adding, then subtracting δr on the 2nd iteration enlarges the basin of the smaller fixed value (solid curve), while the bigger fixed value appears more stable in the other phase (dashed line).

The modulation can eliminate two of the three (period-one is still present) fixed points as can be seen as follows: $x_{n+2}=x_n\Leftrightarrow f(f(x,r_1),r_2)=x\Leftrightarrow 1=r_1\cdot r_2\cdot(1-x)\cdot[1-r_1\cdot x\cdot(1-x)]\Leftrightarrow x^3+a_1\cdot x^2+a_2\cdot x+a_3=0$, with $a_1=-2$, $a_2=(1+r_1)/r_1$, and $a_3=(1-r_1r_2)/r_2r_1^2$. This third order polynomial has three real distinct roots if the discriminant $D=Q^3+R^2<0$, where $Q=(3a_2-a_1^2)/9$, and $R=(9a_1a_2-27a_3-2a_1^3)/54$. Therefore, the threshold for δr causing a phase jump can be found by solving for the root of the discriminant, $D=D(r_1,r_2)=D(\delta r)$, with $r_{1,2}=r_0\pm\delta r$.

Regarding the (unstable) period-one fixed point as the boundary between the two different basins of attraction, the mechanism of stochastic resonance in this particular case can be viewed in the context of a crisis.[21]

The actual signal, i.e., the equivalent of the beat frequency in the experiment, is superimposed by making δr ''time''-dependent: $\delta r\equiv\delta r_n=\delta r_0\sin(2\pi\omega n)$, with frequency $\omega\ll 1$. A plot of the SNR vs noise for a single logistic map displays the typical SR-behavior: a sharp rise to a maximum and a slow decay for greater noise intensities.

B. AESR in the coupled maps

The different nature of the coupling in the coupled map lattice and the coupled oscillators results in significant differences in the limit of low and high coupling. A measure of the qualitatively different coupling is the maximum obtainable kink width, i.e., the number of sites which constitute the domain boundary. While for the time-continuous coupled elements the kink width at least in principle grows proportionally to the coupling strength, the kink width in the coupled map lattice cannot be pushed beyond eight to nine sites. The limited long range correlations in a coupled map lattice effects the maximum achievable SNR. Since the local kink nucleation cannot involve more than sixteen to eighteen sites, the SNR is expected to saturate for more than 32–34 maps. Figure 13 verifies this trend and also displays two curious differences to the case of the coupled Duffing oscillators[3] and the coupled diode resonators:[4] (i) The SNR is significantly enhanced already for very weak coupling strengths ($\epsilon=0.002-0.01$); and (ii) after reaching a plateau which depends on the number of coupled maps, the maximum SNR does not decrease significantly over the available range of coupling values. These two issues will be subject to further investigation. The array enhancement is verified by the coupled map simulations; the maximum achievable SNR for a single logistic map is around 18 dB, the SNR for 32 optimally coupled maps is between 25 and 26 dB. The resulting enhancement of 7.5 dB is significant.

C. Decay rates and speeds for the coupled maps

In order to understand the phase switching process in the coupled map lattice, as before, we study the dynamic properties of kinks in this section. The kink speed as a function of bias for different coupling values is shown in Figure 14. Several key observations can be gathered from this graph. Each curve displays a linear region which is expected from theory; see Eq. (4). The concavity behavior for larger forces (bias) qualitatively agrees well with the nonlinear corrections

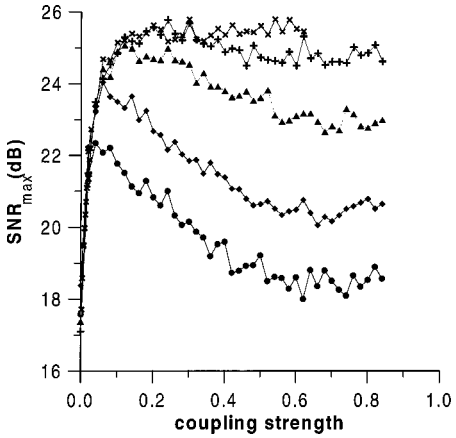

FIG. 13. The maximized SNR vs coupling for different numbers of coupled logistic maps. From top to bottom: $N=32,15,9,5,3$. The parameter $r=3.2$ was chosen such that each individual map is in a stable period two. The signal amplitude is sub-threshold $\delta r=0.04$.

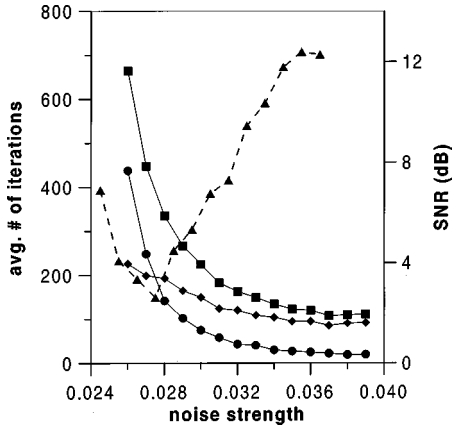

FIG. 15. Average time (# of iterations) it takes to nucleate the 1st kink (circles), then to fully decay (diamonds), the sum (squares) as well as the corresponding SNR (triangles, dashed line) versus applied noise. The minimum SNR results from the crossover of the two time-scales, i.e., when the nucleation time is equal to the subsequent full decay.

obtained in the ϕ^4 theory discussed in Sec. III; see also Eq. (13). Only curves corresponding to coupling values larger than 0.3 go through the origin. For low coupling the discrete nature of the system requires a nonzero force for kink propagation. This finite speed cutoff at low forces increases with decreasing coupling as can be seen in Figure 14.

Unlike in the experiment, it is straightforward in the coupled map lattice to separate the kink–antikink pair nucleation from the subsequent spreading through the entire array. We expect the nucleation process to have an exponential dependency on the noise strength while the subsequent decay should be regarded as an almost deterministic process. We measured the average number of iterations it takes to nucleate *one* pair under an applied bias as well as the average time it takes to fully decay into the stable phase *afterwards*. Figure 15 shows these two quantities as a function of noise intensity D along with the sum and the corresponding SNR. The sum will be the most accessible variable to be measured in experiments. It can be considered as the equivalent of the average waiting time for one uncoupled system. With the added spatial dimension it can be nicely dissected into two distinct components corresponding to the two processes described above. The time it takes to nucleate the first kink decreases Φ exponentially with the noise intensity D. As can be seen in Figure 15, the subsequent decay time is a slowly decreasing function of the noise, which implies that the (anti)kinks propagate faster for increasing noise. This effect is discussed and utilized in more detail in a forthcoming publication.[22] We plot the SNR on the same graph to illustrate a curious phenomenon: the minimum of the SNR is assumed at almost exactly the noise level where the two time-scales cross. The universality of this coincidence is still a topic of ongoing research.

In order to stay close to the experiment we also measured the half time for the coupled maps. Figure 16 is the equivalent of Figure 10 for the coupled map lattice. The measurement procedure is identical to the experiment: A step force (bias) of -0.01 is applied at time zero to the coupled maps initially being in the less favorable phase. We then measure the number of iterations it takes for half the maps to decay into the stable phase.

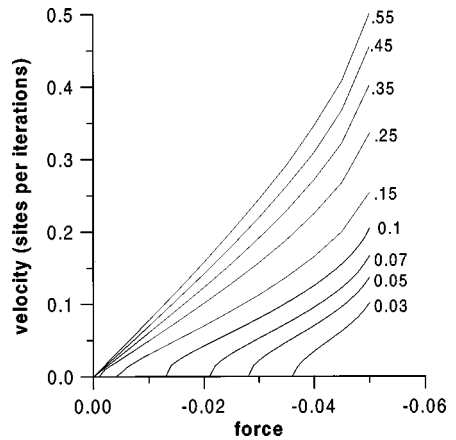

FIG. 14. The same as Fig. 9 for the coupled map lattice. Shown are the kink speeds for different values of the coupling parameter (labeling the curves) as a function of applied bias/force.

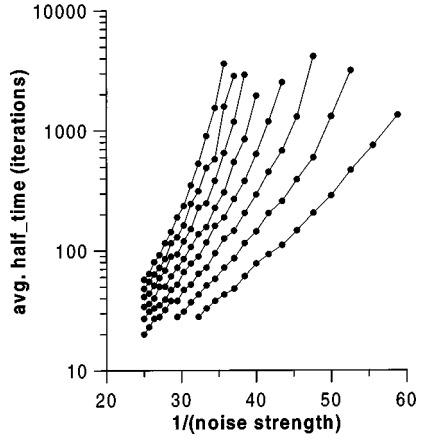

FIG. 16. The same as Figure 10 for the coupled map lattice. The coupling values (increasing upwards) are $\epsilon=0.05$, 0.1, 0.15, 0.2, 0.25, 0.3, 0.35, 0.4 ($r=3.2$, $\delta r=0.01$).

VI. SIGNAL PROCESSING USING COUPLED NONLINEAR DYNAMIC ELEMENTS

In Sec. II, we discussed the enhancement of the response (quantified via an output SNR) of a single stochastic resonator, when it is coupled into an array. We have seen how significant enhancements in the output SNR are possible within well-defined regimes of the noise-coupling parameter space.[4,8] However, in practical scenarios, the SNR is often not the best measure of performance. Indeed, a nonlinear signal processor may output a signal which has infinite SNR but is useless because it has no correlation with the input signal. In practice, therefore, a signal detection system's performance is frequently characterized by measuring its probability of detection and probability of a false alarm. The probability of detection is the probability that a ''decision circuit'' will report that a signal is present when in fact a signal is present. The probability of a false alarm is the probability that the decision circuit will report that a signal is present when in fact a signal is not present. Detection performance can be summarized by receiver operating characteristics (ROCs), which are plots of probability of detection versus the probability of a false alarm.

To illustrate some fundamentals and demonstrate SR-based enhancements in signal processing with *a priori nonlinear* detectors, we consider a very basic signal processing task: detecting a sine wave of known frequency and phase in the presence of Gaussian white noise. One can prove[24] that the best detector for this class of signal consists of an ideal linear filter followed by a ''decision circuit'' which compares the linear filter's output to a threshold. If the filter's output exceeds the threshold, then the system's decision is that the sine wave was present. If we already know what the best detector is, why continue? In practice, there is no such thing as an ideal linear filter. All filters add some noise and deviate from perfect linearity. Our work relates to using coupling to enhance the performance of physically realizable (i.e., nonideal) signal processing elements.

Our decision circuit operates by computing the power spectrum of the waveform of interest (e.g., the input signal, the response of a single isolated element, or the response of an element coupled to $N-1$ other elements) and comparing the power in a narrow frequency band of width $\Delta\omega$ centered at frequency ω to a threshold. If the power exceeds the threshold, the decision circuit concludes that a signal was present. A low threshold leads to high probability of detection and the probability of a false alarm, while a high threshold leads to the low probability of detection and the low probability of a false alarm. To produce a ROC, we repeatedly measure the power in the narrow frequency band and record the value. We do this both with and without the signal actually present. Thus, we obtain power probability distributions for the ''signal''/''no signal'' cases.[9] Using these statistics, the probability of detection for any given threshold power value may be computed by measuring the area under the ''signal'' curve to the right of that value. Similarly, the probability of a false alarm equals the area under the ''no signal'' curve to the right of the threshold value.

In recent work,[9,23] we have computed the ROC curves for the linearly coupled N-element Duffing array introduced in Ref. 3. For this system, the dynamics of the i^{th} element can be cast in the form

$$\begin{aligned}
&\dot{x}_i = kx_i - k'x_i^3 + A\ \sin\ \omega t + N_i(t) + C_i(\epsilon),\\
&C_i(\epsilon) = \epsilon(x_2 - x_1), \quad i=1,\\
&\qquad = \epsilon(x_{i+1} - 2x_i + x_{i+1}), \quad 1<i<N,\\
&\qquad = \epsilon(x_{i-1} - x_i), \quad i=N,
\end{aligned} \tag{18}$$

as well as for a somewhat different system:[7]

$$C_i\dot{x}_i = -\frac{x_i}{R_i} + \sum_{j=1}^{N} J_{ij}\ \tanh\ x_j + A\ \sin\ \omega t + N(t). \tag{19}$$

Systems of the form (19) have been used as continuum analogs of connectionist type electronic neural networks. In such networks, x_i denotes the i^{th} neuron's activation function (membrane potential), and C_i, R_i denote the neuronal input capacitance and trans-membrane resistance, with the coupling coefficients (synaptic efficacies) usually determined via a ''learning rule.'' Here, we shall choose the couplings to maximize the SNR of the response of oscillator $i=1$. This system differs from the previously considered system (18) in that (a) the noise is external (i.e., all elements are driven by an identical noise time series), (b) the coupling is nonlinear, (c) the coupling is global, and (d) a hyperbolic tangent function is used for the nonlinearity. However, the two systems share a wide range of qualitatively similar SR phenomena. In both cases, we see[9,23] a significant enhancement in signal detection for the array compared to the single element. Signal detection is, however, the best when one computes the ROCs directly for the input signal, so why bother with SR? The problem is to acquire the input signal perfectly. If the transducer which picks up the input signal has a perfectly linear response, then it is ideal for our task of detecting a sine wave in Gaussian white noise. If the transducer has a nonlinear (assumed bistable here) response, then coupling it into an array can improve signal detection. Indeed, there exist special cases for which the nonlinearities [the $\tanh\ x_i$ terms in (19)] identically cancel, giving the system a perfectly linear response to its input. For example, this occurs for a pair of identical oscillators ($N=2$, $C_1=C_2$, $R_1=R_2$, $J_{11}=J_{22}$) with couplings $J_{12}=J_{21}=J_{11}$ and identical initial conditions.

It is worth noting that the ROC curves can be predicted directly from the output SNR. Since we do our signal detection by comparing the power in the signal bin of the FFT to a threshold, and since one bin of the FFT covers a very narrow range of frequencies, the noise spectrum across the bin and in the vicinity of the bin looks approximately constant. Therefore we can approximately model the output of our nonlinear array (which supplies the input to the optimal detector) as a sine wave in white noise with a SNR equal to the array's output SNR, R. For this input, the optimal detector's probability of detection (for a set false alarm probability P_{FA}) is[24]

$$P_{\text{D}} = Q(\sqrt{2R}, \sqrt{-2\ln\ P_{\text{FA}}}), \tag{20}$$

where

$$Q(\alpha,\beta)\equiv\int_{\beta}^{\infty} z\,\exp\left(-\frac{z^2+\alpha^2}{2}\right)I_0(\alpha z)dz \tag{21}$$

is Marcum's Q function, and I_0 is the modified Bessel function of the first kind and order zero. This approximating model gives highly accurate results except in a transitional noise range (at low noise strength) where both intra- and interwell motion contribute significantly to the output SNR. The response is most strongly nonlinear in this regime. For example, in this regime turning on the sine wave signal (with input noise strength held constant) causes a large increase in both signal *and* noise output power. In this case, calculations based on just the final value of the output SNR (with the sine wave turned on) underestimate the signal detection performance.

Before concluding, a few words about the output vs input SNR are in order. The optimal detector of a known signal in Gaussian white noise is the correlation receiver or matched filter, which is a linear filter whose output is compared to a threshold. The optimal estimator of a linearly modulated signal in Gaussian white noise is also a linear filter. This suggests why the output of a stochastic resonator circuit driven by Gaussian white noise has an output SNR bounded by the SNR obtained by a linear filter, or, equivalently, the input SNR. Indeed, for a small signal and noise it is easy to prove that the output SNR of any nonlinear system is bounded by the output SNR of the linear filter (or input SNR).

On the other hand, the output SNR of a nonlinear filter may exceed its input SNR under special circumstances. The bandpass limiter is a circuit which illustrates this effect. It consists of a bandpass filter followed by a threshold (or ''infinite limiter'') circuit. The bandpass filter removes all signals outside a narrow band of interest, and the threshold circuit converts the analog output of the bandpass filter to a two-level output ($+V$ if the bandpass filter output is positive, $-V$ if negative). This nonlinear device improves the SNR of a signal by tacitly assuming that the signal power exceeds the noise power. When the assumption holds, the SNR increases by several dB. However, when the assumption fails, the SNR decreases slightly. The fact that there is a positive SNR gain only above a certain threshold input SNR (the ''threshold effect'') is a universal phenomenon generic to all nonlinear processors.[24]

We conclude this section with a few sweeping remarks. We have considered in detail locally, linearly coupled damped nonlinear oscillators subject to local noise, as well as globally, nonlinearly coupled model neurons subject to global noise. We have not found great differences attributable to the particular choice of nonlinearity, nor global vs local coupling. However, linear vs nonlinear coupling and global vs local noise can make a great deal of difference in certain cases. For example, linear coupling has little to no effect on identical oscillators subject to global noise; nor does the summing of outputs. However, as remarked above, nonlinear coupling can completely remove oscillator nonlinearities for some configurations of identical oscillators subject to global noise.

The issue of local vs global noise deserves further comment since it determines whether the noise at different elements of the array is correlated or uncorrelated. If the noise comes from sources internal to the system, then using many elements which are coupled and/or have summed outputs will enhance output SNR, compared to using only one element. In the case of summed outputs, and to some extent in the case of coupling, this is because signal components add coherently, while uncorrelated noise components add incoherently. In the external-noise case, one does not have this effect to exploit, but, somewhat surprisingly, coupling can still enhance output SNR.[7] The external/internal noise distinction also affects how we can measure SNR enhancement. If we are considering the external noise situation, then there is a well-defined input signal plus noise. We can compare the input and output SNR to determine if the system provides any gain in SNR. We can also look at output SNR as a function of N, the number of elements in our array. For internal noise, the input SNR is infinite, because the signal comes into the system with no noise added to it. However, we can still look at output SNR enhancement as a function of N.

VII. CONCLUSION

Stochastic Resonance, when carefully invoked, can enhance the response of an *a priori nonlinear* detector. This enhancement appears to occur for a variety of combinations (linear/nonlinear, local/global, etc.) of coupling and noise scenarios. In this work, we have considered only cyclic and sub-threshold (i.e., there is no deterministic switching) signals; for supra-threshold signals, a variety of other nonlinear effects come into play, and the output SNR can actually exceed that at the input. The SR scenario envisions the noise-assisted *inter*well or hopping motion as the primary carrier of information through the system; intrawell motion is neglected. The maximization of the output SNR has been shown[3,8] to be directly the result of spatio-temporal synchronization of the array dynamics to the external signal. This synchronization, which leads to scaling relationships[8] that can be addressed in the framework of a continuum ϕ^4 field theory of kink–antikink nucleation,[5] has been demonstrated in the experiments[4] that are reviewed in this work.

It should be emphasized that the occurrence of AESR in such a diversity of systems (coupled map lattice, ϕ^4 model, coupled resonators, coupled ODE's) gives strong evidence for its universal nature. Unlike the elements in the numerical simulations, the resonators in the experimental setup were far from identical. Crucial parameters, such as energy barriers or local noise intensities varied significantly. The relatively strong coupling serves to smooth out these inhomogeneities and approach the continuum limit. The absence of coupling induced long-range spatial correlations in the coupled map lattice and its resulting limitations for SR enhancement agrees well with the proposed mechanism of kink–antikink nucleation.[5]

Beyond the tantalizing implications of this collective behavior in biological neural networks and bioengineering receptors, for example, the practical problem of exploiting SR and AESR in signal detection scenarios has recently attracted

a fair amount of attention; some aspects of this problem have been reviewed (Sec. VI). The starting point is the precept that even when the detector is nonlinear, a knowledge of the signal detection statistics and their behavior under the conditions of SR is essential before one can consider a practical implementation. We have demonstrated that there exists an optimal noise value at which the detection probability (for a fixed false alarm rate) is a maximum. This idea is being applied to sophisticated signal detection scenarios[25] involving SR in real-world detection systems, wherein the number of adjustable parameters is increased over simple or ''classical'' SR applications. In these systems, an improper choice of parameters (or operating points) can easily degrade the signal detection properties; this lends credence to the maxim that the *quantitative* dynamics of a particular nonlinear device have to be fully understood before one can hope to apply it to real-world situations, despite the fact that the qualitative behavior of nonlinear dynamic systems may be generically similar.

ACKNOWLEDGMENTS

Much of the research described in this review has been supported by the Physics Division of the Office of Naval Research; it is a pleasure to thank them for their support. In particular, ML, DC, and ERH were supported under Grant No. N0014-94-1-0395. ARB and MEI would, further, like to acknowledge support from the Internal Research program at SPAWAR Systems Center, as well as a NATO CRG 131464.

[1] K. Wiesenfeld and F. Moss, Nature (London) **373**, 33 (1995); L. Gammaitoni, P. Hänggi, P. Jung, and F. Marchesoni, Rev. Mod. Phys. **70**, 223-288 (1998).
[2] R. Benzi, A. Sutera, and A. Vulpiani, J. Phys. A **18**, 2239–2245 (1985).
[3] J. F. Lindner, B. K. Meadows, W. L. Ditto, M. E. Inchiosa, and A. R. Bulsara, Phys. Rev. Lett. **75**, 3 (1995).
[4] M. Löcher, G. A. Johnson, and E. R. Hunt, Phys. Rev. Lett. **77**, 4698 (1996).
[5] F. Marchesoni, L. Gammaitoni, and A. R. Bulsara, Phys. Rev. Lett. **76**, 2609 (1996).
[6] P. Jung, U. Behn, E. Pantazelou, and F. Moss, Phys. Rev. A **46**, R1709 (1991); A. Bulsara and G. Schmera, Phys. Rev. E **47**, 3734 (1993); M. Inchiosa and A. Bulsara, Phys. Lett. A **200**, 283 (1995); P. Jung and G. Mayer-Kress, Phys. Rev. Lett. **74**, 2130 (1995); A. R. Bulsara and L. Gammaitoni, Phys. Today **49**, 39–45 (March 1996); J. J. Collins, C. C. Chow, and T. T. Imhoff, Nature (London) **376**, 236 (1995); P. C. Gailey, A. Neiman, J. J. Collins, and F. Moss, Phys. Rev. Lett. **79**, 4701 (1997).
[7] M. Inchiosa and A. Bulsara, Phys. Rev. E **52**, 307 (1995).
[8] J. F. Lindner, B. K. Meadows, W. L. Ditto, M. E. Inchiosa, and A. R. Bulsara, Phys. Rev. E **53**, 2081 (1996).
[9] M. E. Inchiosa, A. R. Bulsara, J. F. Lindner, B. K. Meadows, and W. L. Ditto, in *Proceedings of the Meeting on Nonlinear Dynamics and Full Spectrum Processing*, edited by R. A. Katz, AIP Conf. Proc. (American Institute Physics, New York, 1995).
[10] R. W. Rollins and E. R. Hunt, Phys. Rev. Lett. **49**, 1295 (1982).
[11] W. Yang, M. Ding, and G. Hu, Phys. Rev. Lett. **74**, 3955 (1995); H. L. Yang, Z. Q. Huang, and E. J. Ding, Phys. Rev. E **54**, R5889 (1996).
[12] G. A. Johnson, M. Löcher, and E. R. Hunt, Phys. Rev. E **51**, R1625 (1995); Physica D **96**, 367–437 (1996).
[13] F. Marchesoni, C. Cattuto, and G. Costantini, Phys. Rev. B **57**, 7930 (1998), and references therein.
[14] J. F. Currie, J. A. Krumhansl, A. R. Bishop, and S. E. Trullinger, Phys. Rev. B **22**, 477 (1980).
[15] J. S. Langer, Ann. Phys. (N.Y.) **54**, 258 (1969); see also G. Callan and S. Coleman, Phys. Rev. D **16**, 1762 (1977).
[16] P. Hänggi, F. Marchesoni, and P. Sodano, Phys. Rev. Lett. **60**, 2563 (1988).
[17] F. Marchesoni, Ber. Bunsenges. Phys. Chem. **95**, 353 (1991).
[18] *Temperature* is defined as the square of the rms voltage of the noise sources.
[19] W. H. Press, S. A. Teukolsky, W. T. Vetterling, and B. P. Flannery, *Numerical Recipes in C*, 2nd ed. (Cambridge University Press, Cambridge, 1992).
[20] P. M. Gade, R. Rai, and H. Singh, Phys. Rev. E **56**, 2518 (1997).
[21] T. L. Carroll and L. M. Pecora, Phys. Rev. Lett. **70**, 576 (1993).
[22] M. Löcher, D. Cigna, and E. R. Hunt, Phys. Rev. Lett. **80**, 5212 (1998).
[23] M. Inchiosa and A. Bulsara, Phys. Rev. E **53**, R2021 (1996).
[24] H. van Trees, *Detection, Estimation and Modulation Theory* (Wiley, New York, 1978).
[25] M. Inchiosa and A. Bulsara, Phys. Rev. E **58**, 115 (1998).